Computers in Biology and Medicine 114 (2019) 103422

Contents lists available at ScienceDirect

Computers in Biology and Medicine

journal homepage: http://www.elsevier.com/locate/compbiomed

Multiscale connected chain topological modelling for microcalcification classification

Minu George [a,*], Zhili Chen [b], Reyer Zwiggelaar [a]

[a] Department of Computer Science, Aberystwyth University, SY23 3DB, UK
[b] School of Information and Control Engineering, Shenyang Jianzhu University, Shenyang, 110168, China

ARTICLE INFO

Keywords:
microcalcification
Topological modelling
Multiscale connected chains
Benign/malignant classification

ABSTRACT

Computer-aided diagnosis (CAD) systems can be employed to help classify mammographic microcalcification clusters. In this paper, a novel method for the classification of the microcalcification clusters based on topology/connectivity has been introduced. The proposed method is distinct from existing techniques which concentrate on morphology and texture of microcalcifications and surrounding tissue. The proposed approach used multiscale morphological relationship of connectivity between microcalcifications where connected chains between nearest microcalcifications were generated at each scale. Subsequently, graph connectivity features at each scale were extracted to estimate the topological connectivity structure of microcalcification clusters for benign versus malignant classification. The proposed approach was evaluated using publicly available digitized datasets: MIAS and DDSM, in addition to the digital OPTIMAM dataset. The classification of features using KNN obtained a classification accuracy of $86.47 \pm 1.30\%$, $90.0 \pm 0.00\%$, $82.5 \pm 2.63\%$, $76.75 \pm 0.66\%$ for the DDSM, MIAS-manual, MIAS-auto and OPTIMAM datasets respectively. The study showed that topological/connectivity modelling using a multiscale approach was appropriate for microcalcification cluster analysis and classification; topological connectivity and distribution can be linked to clinical understanding of microcalcification spatial distribution.

1. Introduction

Breast cancer remains the most common cause of cancer deaths among women worldwide [1]. The best way to reduce the mortality rate is early detection and treatment at an appropriate time. Mammography remains the most effective primary imaging tool for monitoring and detection of abnormalities in breast tissue [2]. Mammography helps in identifying abnormalities before they provide physical symptoms thus giving a higher chance of treatment at an earlier stage [3]. Types of abnormalities detected in mammograms are masses, micro-calcifications and architectural distortions. These are classified as malignant based on certain characteristics like size, shape, form, number, density, distribution pattern and cluster pattern [2]. Breast microcalcifications are small spots of calcium deposits which are represented as white specks in mammograms [4,5] as shown in Fig. 1. Though most detected microcalcifications are benign, the presence of fine and granular patterned microcalcifications could be an early indication of breast carcinoma requiring further investigation and potentially treatment [4]. Irrespective of all the benefits of mammography, it has limitations which makes the categorization of detected lesions as benign or malignant difficult for radiologists. Since a mammogram is a two-dimensional representation of a three-dimensional breast, during the imaging process it may superimpose breast tissue and ducts producing patterns like abnormal lesions. It could alter the appearance of malignant lesions leading to incorrect assessment [2].

Due to limitations at screening and the number of mammographic images to be diagnosed, approximately 10%–30% of breast cancers present in mammograms are missed or misinterpreted by radiologist either due to technical or visualization problems [6,7]. During the evaluation process differences from normal tissue patterns, architectural distortions, the subtle signs of malignancy are identified [8]. For the malignancy confirmation of microcalcifications found in mammogram, image guided core biopsy using ultrasound with specimen radiography would be performed [9]. In-order to overcome the limitations of assessing large numbers of mammograms through screening programs and to improve the diagnosis accuracy, Computer-Aided Diagnosis (CAD) systems have been developed to assist radiologists [10–14]. Although the efficiency of CAD systems in cancer detection and

* Corresponding author.
E-mail address: mig24@aber.ac.uk (M. George).

https://doi.org/10.1016/j.compbiomed.2019.103422
Received 25 February 2019; Received in revised form 29 August 2019; Accepted 29 August 2019
Available online 5 September 2019

diagnosis is under debate [15], CAD techniques could offer a cost-effective alternative to double reading and it is undergoing a paradigm shift with emerging machine learning methods and advanced deep learning algorithms [16–18]. The clinical interpretation of microcalcification remains a difficult task for CAD systems due to the small size of calcification, low distinguishability from the surrounding dense tissue or overlapping tissues, and the absence of standard patterns or templates [2,19,20].

Microcalcification clusters (MCC) are a primary sign of breast cancer. The clinical characterisation of microcalcification clusters is: no fewer than three microcalcifications in an area of 1 cm^2 [19,21–23] and the spatial resolution of mammography (40–100 μm per pixel) with the size of microcalcifications ranging from 0.1 to 1.0 mm with an average of about 0.3 mm [19,23], indicates that each microcalcification can be several pixels in diameter. Assessment of breast microcalcifications indicates that malignant micro-calcifications tend to be small and densely distributed (>5 per focus within 1 cm^2) while benign micro-calcifications are usually larger, smaller in number and scattered (<4–5 per 1 cm^2) [23]. The presence of fine, patterned granular micro-calcification clusters can be an indication of early breast carcinoma. The uncertainity of accurately predicting malignancy of MCCs leads to unnecessary biopsies and patient stress. CAD systems can play a role in reducing false positive results [24,25].

A variety of MCC characteristics have been used by CAD systems for classification purposes. The features should be reliable, independent, discriminative and limited in number to enhance overall performance and efficiency of the CAD system for classification [26]. The literature has used shape, texture, statistical and cluster features for the classification of abnormalities [26]. For shape features, both individual and cluster shape features have been considered. Shape features, like the size of individual calcification, the number of calcifications in a cluster, the sum of areas of calcifications in a cluster, the maximum value of compactness, the maximum standard deviation, the average roughness, compactness, distribution features, contrast, eccentricity, the relative distance from the pectoral muscle, shape orientation features, average size per calcifications, irregularity, elongation, border gradient strength, local contrast, central moment, and calcification area have been the most common features extracted for classification [21,27–30]. Statistical features like surrounding region dependence (SRD), spatial grey-level dependence (SGLD), grey-level run length (GLRL), grey-level difference (GLD) have been used for extracting contrast, entropy, angular second moment (energy), correlation, difference variance, inverse difference moment, skewness, kurtosis, and intensity ratio for the classification of abnormalities [30–33]. Similarly, multiscale texture features have been extracted using variants of wavelets with various scaling functions [21,34–36] and fractal methods [37,38]. Recently, deep learning techniques have been developed for detection and for classifying the lesions in mammograms [39–42].

Chen et al. [43,44] evaluated the topology of microcalcification clusters by constructing graphs at multiple scales and was unlike existing approaches which had concentrated on individual microcalcification morphology. Subsequently, a multiscale topological feature vector with subgraph features and average degree of nodes were investigated. The robustness of the method and effect of dataset size was evaluated by selecting samples at multiple scales for classification of clusters into benign and malignant cases. Similarly, Suhail et al. [45] used a tree based topological approach for the classification of microcalcification focusing on the distribution and connectivity of microcalcification. Features like the height of the tree and the number of leaf nodes were evaluated for the classification process. Topology-based classification showed the potential of topological and distribution features of microcalcification in mammogram for abnormality classification.

Our project explores the topological and distributional connectivity of microcalcifications for classifying the abnormality as benign or malignant. To make the method robust with respect to the size of the microcalcifications and the distribution within the clusters, a multi-scale approach was employed. The proposed method utilizes the closeness and topology of microcalcification in representing clusters at multiple scales.

2. Data

The data used for the evaluation was from two publicly available database: the Digital Database for Screening Mammography (DDSM) [46] and the Mammographic Image Analysis Society (MIAS) database [47], from which relevant regions of interest (ROIs) were extracted for evaluation. The mammograms from the Digital Database for Screening Mammography (DDSM) were digitized by either of four scanners; DBA M2100 ImageClear (42 μm per pixel, 16 bits), Lumisys 200Laser (50 μm per pixel, 12 bits), Howtek MultiRad 850, Howtek 960 (43.5 μm per pixel, 12 bits). The BIRADS classification for stages of malignancy and benign cases were provided by expert radiologist and were available as part of the database. A total of 289 mammogram patches of varied sizes with microcalcifications from DDSM were evaluated, where 131 mammographic patches were reported as malignant cases while 158 mammographic patches were marked as benign cases. All the microcalcification clusters in the images were histologically confirmed. The average size of these patches was 482 × 450 pixels though the proposed method worked independent of the patch size. The automatic detection of microcalcifications was done using the segmentation approach developed by Oliver et al. [48]. Oliver's detection method estimated all the morphological features of individual microcalcifications using local image features which was then trained by a pixel-based-boosting classifier to select the most salient features. Thereafter, the microcalcfication clusters were estimated based on the local neighbourhood for each microcalcifications detected from the previous stage as shown in Fig. 1.

Similarly, mammographic ROIs from the MIAS database were also

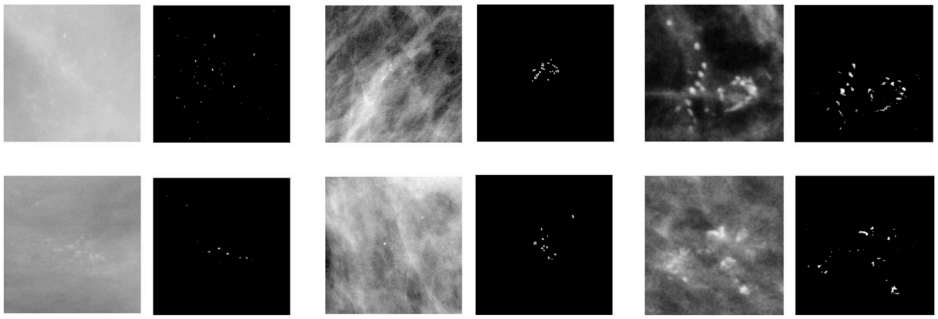

Fig. 1. Examples of ROI patches of malignant (top row) and benign (bottom row) mammographic microcalcification clusters from MIAS and DDSM dataset, First column: original patch from DDSM; second column: segmented microcalcifications; third column: original patches from MIAS; fourth column: segmented microcalcifications, fifth column: original patches from OPTIMAM; sixth column: segmented microcalcifications.

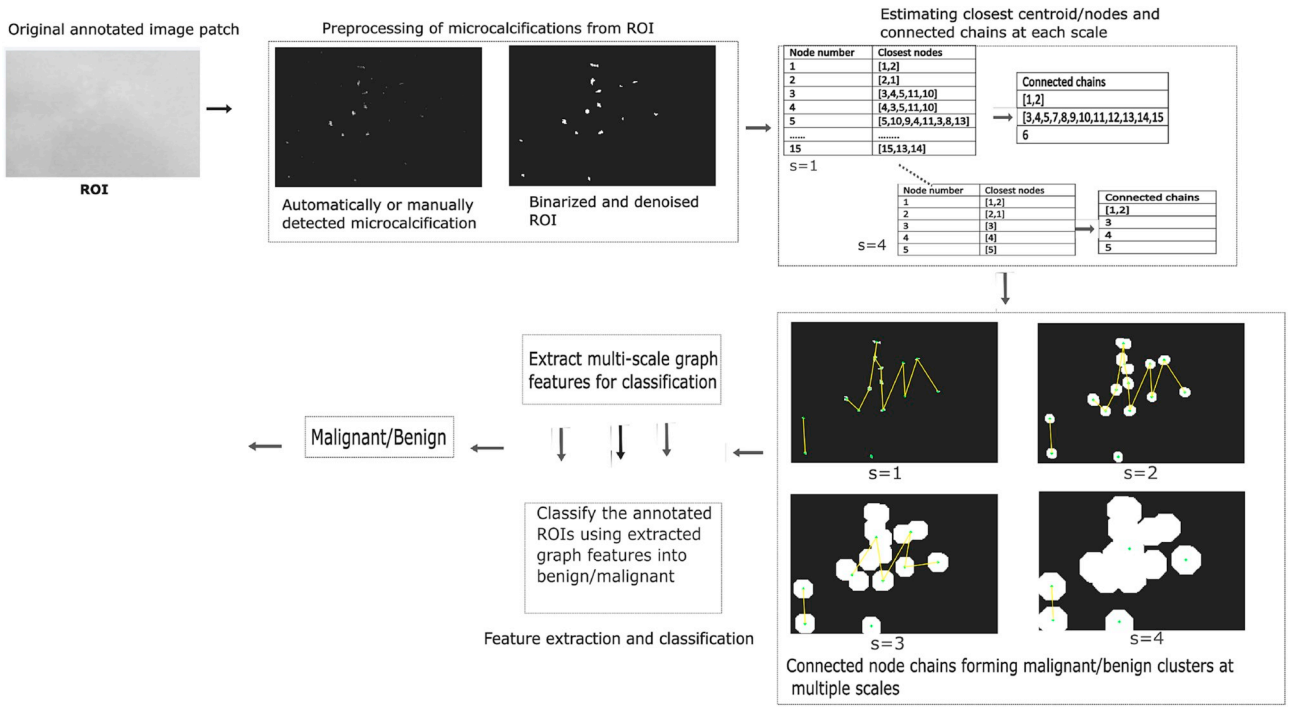

Fig. 2. Detailed representation of the proposed multi-scale connected chain graph method for benign/malignant microcalcification classification.

used for the evaluation process. The MIAS database contains 322 digitized mammograms of 161 women. Each image was digitized to 50 μm pixel edge with a Joyce-Loebl scanning microdensitometer representing each pixel with an 8 bit grey-level. Image ROIs with microcalcification clusters were extracted with an image patch size of 512 × 512 pixels. There were in total of 20 images in the MIAS dataset containing microcalcification cluster ROIs with 11 benign clusters and 9 malignant cases which were all categorised by histology. In order to estimate the effect of MC cluster segmentation for the proposed classification method, MC's in ROIs where also manually annotated (MIAS-manual) in addition to segmentation (MIAS-auto) by the method developed by Oliver et al. [48].

In addition to DDSM and MIAS, the digital dataset OPTIMAM was used. The database is being developed. More information on the OPTIMAM database can be seen from 'http://commercial.cancerresearchuk.org/optimammammography - image-database-and-viewing-software'. In the proposed method, 286 mammographic images with microcalcification clusters were used for estimating the robustness of the algorithm, where 136 ROIs were histologically reported as benign and 150 were categorised as malignant. The microcalcifications were segmented using the detection approach developed by Alam et al. [49]. The extracted RoIs are initially enhanced using a wavelet-based algorithm. The segmentation of microcalcifications were then done through applying a sequence of interpolation and morphological operations on the enhanced RoIs. The entire RoI image was divided into sub-regions and a bi-cubic interpolation method was applied to obtain the intensity level of the local background. Then a series of morphological operations were used to reduce the over segmentation. In addition, to reduce the false positive responses, the image was divided into 100 × 100 blocks, and if a block contained fewer than 3 objects those objects were removed.

3. Proposed methodology

The proposed approach is based on the clinical perception of the distribution and morphology of microcalcifications. It has been observed that benign microcalcifications are of larger size and distributed widely compared to malignant cases with smaller and closely distributed microcalcifications. The proposed methodology used automatically or manually segmented microcalcifications in patches as the input which were binarized and denoised for the classification process. The closeness of microcalcifications in ROIs was estimated through connected chain graphs at different scales followed by the extraction and classification of connected chain graph features at respective scales for malignant or benign classification. A detailed description showing each step of the process (using an image from the DDSM with ROI size 152 × 224) is shown in Fig. 2, the pseudo-code is presented in Algorithm 1 and details can be found in subsequent subsections.

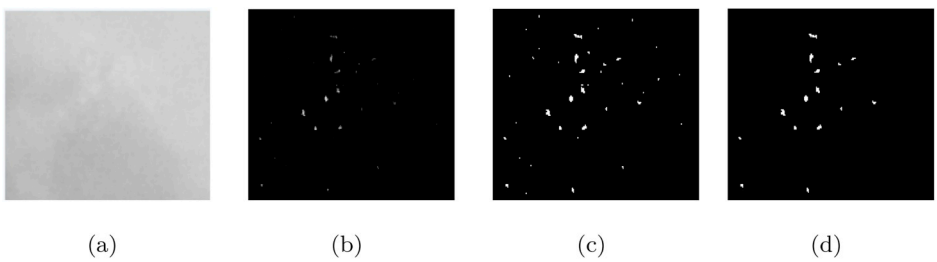

Fig. 3. Binarization and denoising of automatically detected microcalcification cluster; (a) original mammographic patch with microcalcifications, (b) microcalcification cluster image, (c) binarized image, (d) denoised image.

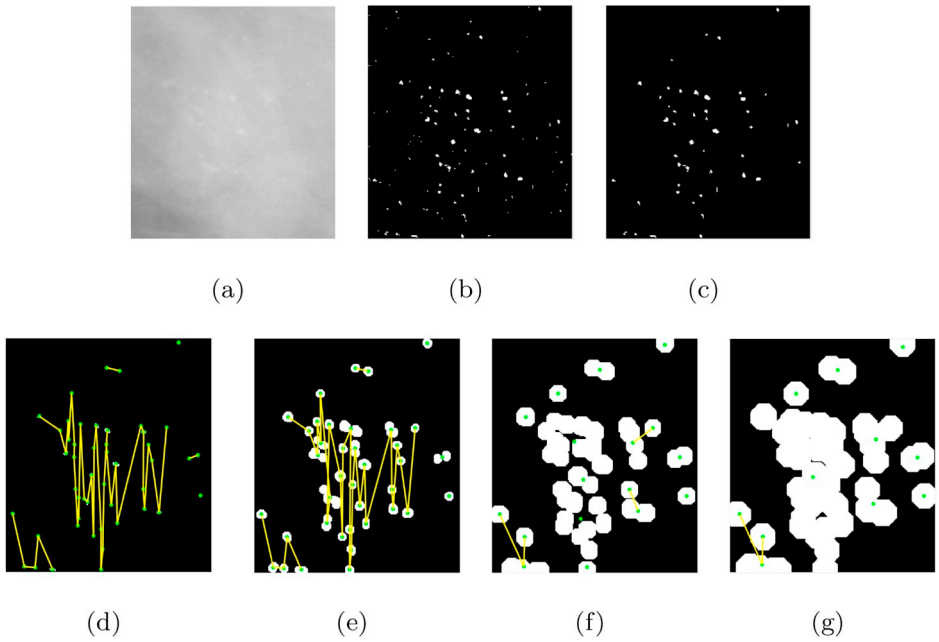

Fig. 4. Connectivity pattern of microcalcifications with morphological dilation at increasing scales. (a) original image ROI, (b) segmented microcalcification mammographic ROI, (c) connected chains at scale 1, (d) connected chains at scale 2 (microcalcifications have started merging), (e) connected chains at scale 3 (most of microcalcifications have merged), (f) connected chain at scale 4 (majority of microcalcifications overlapped forming a single unit).

Pre-processing. The automatically or manually segmented mammographic ROIs are binarized for further morphological operations. The pixels representing the abnormal tissue from the segmented ROIs are represented with a pixel value '1′ and normal tissue or background is using pixel value '0' after using a probability threshold of luminence level of 0.3. Denoising is performed on the binary image by removing regions which are less than 4 pixels in size considering those as noise or as low probability microcalcification regions. The binarization and pre-processing procedures are demonstrated in detail (using an image from the DDSM with ROI size 152×224) in Fig. 3.

Constructing Connected Chains at Multiple Scales. Following denoising, the centroid of each microcalcification was calculated for finding the nearest microcalcifications. Initially, all centroids were considered as independent nodes. The number of scales was set (e.g. $S = 4$). We selected S equal to four because a large scale number with large structuring element for dilation can morphologicaly merge all the microcalcifications at an early stage making it a single unit. At each scale a morphological dilation operation using a disc shaped structuring

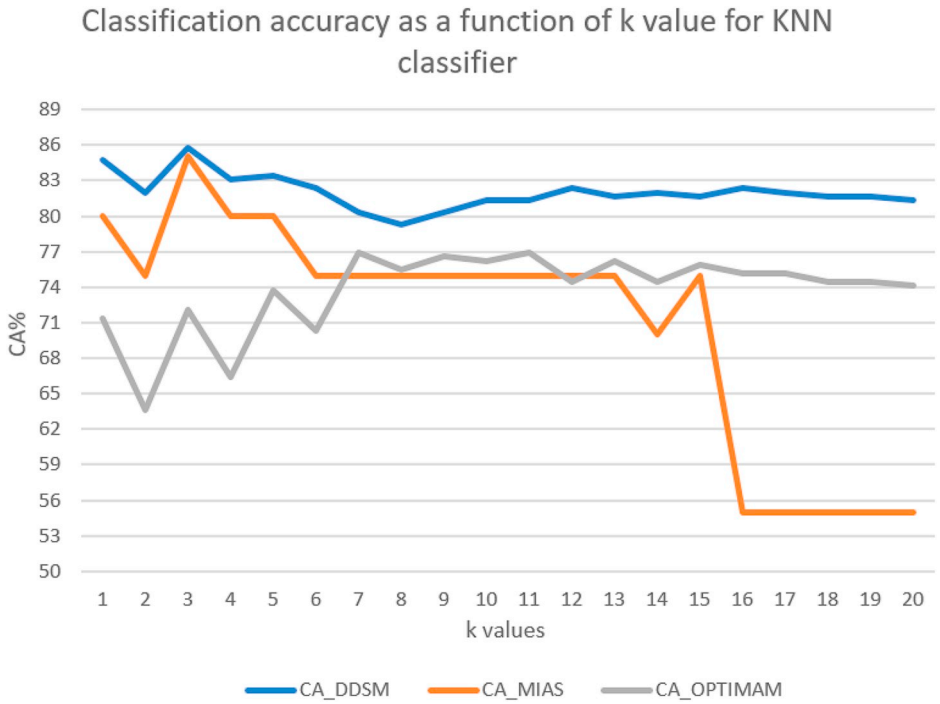

Fig. 5. Variation of classification accuracy (CA%) with k-values for KNN classifier (The dotted line shows the trendline of classification accuracy with-respect to k values).

element with radius size of 5 pixels was performed for estimating the connectivity between microcalcification centroids. Similarly, reducing the size of the structuring element would need additional scales to merge the microcalcifications.

The distance between each centroid point was calculated to estimate the closeness in distribution at each scale generated by each distance map. Subsequently, connected chains were generated to describe the morphological distribution of each microcalcification with respect to other microcalcifications. For the first scale, nodes were connected which were distributed within a threshold distance of 40 pixels (an approximate threshold distance when 1 cm distance translated based on resolution). The Euclidean distance measure [50] was used for distance calculations. A distance map was created representing all the microcalcifications (by node number) in the denoised patch and the nodes which were in the range of the threshold distance to each microcalcification (mentioned as the closest nodes). To generate the connected chain pattern, the initial node from the distance map was selected as the first node in the chain. The closest node to it from the list was connected to it, followed by connecting the closest node to the lastly connected node till all the closest nodes in the visted node list were connected. The procedure continued by selecting the next unvisited node (from the node number list) to start the next chain. The procedure is repeated recursively until all the nodes were visited and connected. So, each connected chain represented a sub-cluster of microcalcification. For the next scale, morphological dilation [51] using a disk structural element of size 5 was performed on the binary microcalcifications and the centroids and distance map were calculated followed by the connected chain estimation. The chain generation procedure is repeated for all the scales using a disc structuring element incremented by size 5.

The connected chains at each scale represented the arrangement or pattern of microcalcification in the clusters. The connected chains structure differed with each scale as some dilated microcalcifications merged giving a single centroid for distance estimation. The closely distributed microcalcifications merged at the initial stages of dilation forming a single unit. Therefore, the morphological dilation process gave different connectivity patterns between the microcalcifications forming different independent sub-clusters. The detailed scale space clustering is illustrated in Fig. 4. Since the malignant microcalcifications were closely located, with increasing scales they tended to merge early as a region while the benign microcalcifications needed additional scales to be united as they were more diffusely distributed.

Feature extraction. In the connected chain each node is the centroid of a microcalcification and is considered independent. It is noted that the number of connections between nodes decreased with increasing scales as the microcalcifications started merging. The graph features of the connected chains at each scale were extracted and concatenated to form the feature vector for classification. The cluster properties calculated at each scale were the number of clusters, the benign clusters (the chains containing less than 5 nodes), the number of malignant chains (the chains with more than 5 nodes), the size of the longest chain, the number of independent nodes/leaf nodes.

Classification. The classification of mammographic patches into benign or malignant using the connected chain features at different scales was performed using classical k nearest neighbour (kNN) [52] on the MIAS, DDSM and OPTIMAM databases. The classical kNN classifier is an instance based learning approach [52]. We selected the kNN classifier as most of the literature used the classical kNN approach although it should be clear that alternative classifiers are possible. The kNN classifier was based on simple majority voting unless equal class probability were indicated and the Euclidean weighted approach was used as the distance measure. The features extracted from each scale as mentioned before were fed into a kNN classifier.

Table 1
Confusion matrices for automatic classification using a kNN classifier for 10-FCV (CA = 87.88%) and leave-one-out (CA = 87.54%) approaches for DDSM.

		Automatic Classification			
		10 -FCV		Leave-one-out	
		Benign	**Malignant**	**Benign**	**Malignant**
Truth Data	**Benign**	149	9	148	10
	Malignant	26	105	26	105

Table 2
Confusion matrices for automatic classification using a kNN classifier for 10-FCV (CA = 85.0%) and leave-one-out (CA = 80.0%) approach for MIAS-auto and 90.0% for MIAS-manual.

		Automatic Classification			
		10 -FCV		leave-one-out	
		Benign	**Malignant**	**Benign**	**Malignant**
Truth Data, MIAS-auto	**Benign**	10	1	10	1
	Malignant	2	7	3	6
Truth Data MIAS-manual	**Benign**	10	1	10	1
	Malignant	1	8	1	8

Table 3
Confusion matrices for automatic classification using a kNN classifier for 10-FCV (CA = 77.27%) and leave-one-out (CA = 77.27%) approach for OPTIMAM.

		Automatic Classification			
		10-FCV		leave-one-out	
		Benign	**Malignant**	**Benign**	**Malignant**
Truth Data	**Benign**	99	37	99	37
	Malignant	28	122	28	122

Algorithm 1. Multi-scale connected chain algorithm

Input: Automatically or manually segmented microcalcification cluster RoIs, threshold distance, number of scales

Output: Multi-scale connected chain features to classify microcalcification clusters as benign or malignant.

1: Binarize and denoise the image to remove low probability microcalcification regions from RoI
2: Compute the centroids of each microcalcifications considering them as independent nodes of the chain
3: **for** scale less than 5 **do**
4: Generate a distance map by computing the closest nodes to each node based on the threshold distance.
5: **for** scan each node in the distance map node-list **do**
6: Merge the closest node to each node in distance map to form a chain till all nodes in the node list are visited
endFor
7: Extract the chain features from each scale like number of independent nodes in each scale, number of malignant chains (chains with more than 5 nodes), number of benign nodes (chains with less than 5 nodes) and the size of longest chain.
8: Increment the scale number
9: Dilate the microcalcification objects in RoIs using a disc structuring element of size 5 pixels
endFor
10: Generate the feature vector for classification by merging the features extracted at different scales.

Table 4
The classification accuracy fro MIAS, DDSM and OPTIMAM datasets for 10 run 10-FCV and leave-one-out approaches.

		CA	
		10-FCV	**Leave-one-out**
Dataset	**MIAS-auto**	82.50% ± 2.63%	80.0%
	MIAS-manual	90.00% ± 0.00%	90.0%
	DDSM	86.47% ± 1.30%	87.5%
	OPTIMAM	76.75% ± 0.66%	76.9%

Table 5
The area under the ROC curve for the MIAS, DDSM and OPTIMAM datasets for 10 run 10-FCV and leave-one-out approaches.

		A_z	
		10-FCV	**Leave-one-out**
Dataset	**MIAS-auto**	0.848 ± 0.013	0.83
	MIAS-manual	0.899 ± 0.000	0.89
	DDSM	0.899 ± 0.008	0.90
	OPTIMAM	0.776 ± 0.005	0.78

4. Experimental results and discussion

To evaluate the performance of the proposed methodology, the graph features extracted at different scales were used with a leave-one-out and ten fold cross validation (FCV) approaches on the MIAS, DDSM and OPTIMAM datasets to investigate how significantlty these approaches affected the classification accuracy. We used a kNN classifier with a ten-run ten-fold cross validation scheme to calculate the accuracy of classification on different dataset. In order to find the best k value for the KNN classifier for different datasets, we performed the classification using different k values as shown in Fig. 5. The k value was selected based on the best classification accuracy. An example of the variation of classification accuracy with k values for the DDSM dataset (highest CA% when k = 3) is shown in Fig. 5. The same procedure was applied for the MIAS and OPTIMAM datasets for selecting the k value for the kNN classifier. The best classification results using the kNN (k = 3) classifier on the DDSM dataset is illustrated in Table 1, which shows an average classification accuracy (CA%) of 86.47% ± 5.94% for a 10 run 10 fold cross validation and 87.5% for the leave-one-out approach. (see Table 4). The sensitivity/recall (TP/(TP + FN)) of the test, which measures the ability of the test to correctly identify those malignant cases was found to be 86.76%, a precision of 86.86% with an F-score (to measure the performance of the test for the positive class) of 86.34% for the DDSM dataset.

Similarly, the classification of microcalcifications as benign or malignant for the automatically segmented MIAS dataset using the kNN classifier (k = 3, see Fig. 5) gave a classification accuracy (CA%) of 82.5% ± 2.63% for 10 run 10-FCV and 80.0% for leave-one-out approaches (see Table 2 (for the best classification accuracy) and Table 4). The test results shows a sensitivity of 82.5%, precision (TP/TP + FP) of 82.25% with F-score of 83.05%. In order to estimate the importance of segmentation accuracy in classification, the MIAS ROIs were manually segmented (MIAS-manual). The classification of manually segmented MCs shows a classification accuracy of 90.0% for 10 run 10-FCV and leave-one-out approaches with sensitivity, precision and F-score to be 90.00% respectively.

Subsequently, the classification of microcalcifications as benign or malignant for the OPTIMAM dataset using the kNN classifier (k = 11, see Fig. 5) gave a classification accuracy (CA = (TP + TN)/(TP + TN + FP + FN)) of 76.75% ± 0.66% and 77.27% for 10 run 10-FCV and leave-one-out approaches (see Table 4), respectively. The best classification accuracy for the 10 fold cross validation is illustrated in Table 3. The sensitivity/recall for the classification test for OPTIMAM using the kNN classifiers was found to be 76.68% with a precision (measure of classifiers exactness) of 76.69%, attaining F-score to be 76.63%.

The second evaluation process used for investigating the efficiency of classification was performed by ROC (Receiver Operating Characteristic) under the curve analysis. In our approach, the binary classification,

Table 6
Comparison of our results with those achieved by related work.

Feature	Database	Cases	Classifier	Method	Result
Cluster	MIAS	25	SVM	Papadopoulos et al. [24]	$A_z = 0.81$
Shape	DDSM	183	Threshold	Ma et al. [54]	$A_z = 0.96$
Intensity, shape and linear structures	DDSM	150	ANN/SVM	Ren et al. [55]	$A_z = 0.94$
	MIAS	20	kNN	Ashiru et al. [56]	$A_z = 0.95$
Topology & location					
Topology & location	DDSM	280	kNN	Ashiru et al. [56]	$A_z = 0.75$
	MIAS	322	SVM	Dheeba et al. [57]	CA = 86.1
Law features					
	DDSM	300	kNN	Strange et al. [22]	CA = 80%
Topological features					
	DDSM	300	kNN	Chen et al. [44]	CA = 85.2% ± 5.7%
Topology					
	DDSM	129	Majority voting	Suhail et al. [45]	CA = 91%
Tree-based modelling					
	DDSM	289	KNN	George et al. [58]	CA = 86%
Connected chain model					
Multiscale connected chain	DDSM	289	kNN	Ours	CA = 86.47% ± 1.30% $A_z = 0.892 \pm 0.008$
Multiscale connected chain	MIAS-auto	20	kNN	Ours	CA = 82.5% ± 2.63% $A_z = 0.848 \pm 0.013$
Multiscale connected chain	MIAS-manual	20	kNN	Ours	CA = 90.00% ± 0.00% $A_z = 0.899 \pm 0.000$
Multiscale connected chain	OPTIMAM	286	kNN	Ours	CA = 76.75% ± .66% $A_z = 0.776 \pm 0.005$

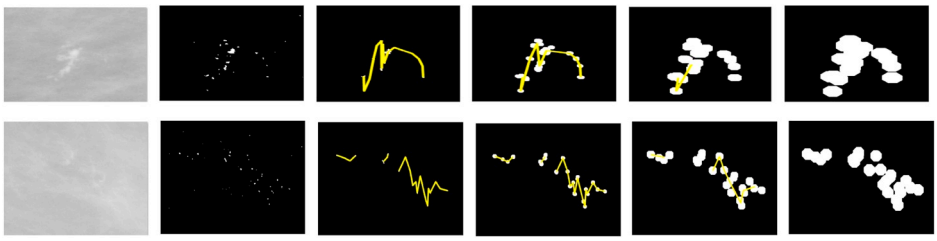

Fig. 6. Misclassified examples. First row: a benign ROI reported as malignant, second row: a malignant ROI reported as benign.

the TPR (True Positive Rate) represented the number of correctly classified malignant cases to the total count of malignant cases. Similarly, the FPR (False Positive Rate) is defined as the number of incorrectly classified benign cases to the total number of benign cases in the dataset. AUC (Area Under the Curve, A_z) is a measure of sensitivity and specificity showing the overall performance of a diagnostic test and is interpreted as the average value of sensitivity for all possible values of specificity [53]. The area under the ROC curve for the three datasets is shown in Table 5 for the 10 run 10-FCV.

While performing a quantitative comparison with alternative state of art methods which used topological methods for microcalcification classification using the DDSM dataset, our results are in-line with the results obtained by Chen et al. [44] using multiscale graph modelling with a classification accuracy (CA%) of 85.2% ± 5.7% for a set of 300 ROIs without feature selection and Suhail et al. [45] with classification accuracy of 91.0% using tree-based modelling on a subset of 129 ROIs from the DDSM dataset. The classification accuracy of our approach was found to be 86.47% ± 1.31% for a set of 289 ROIs from the DDSM dataset. Additional comparison of our results with those achieved by other related work with the same datasets are shown in Table 6.

In addition to the KNN classifier, a 10 FCV was done using a SVM classifier and this obtained a CA equal to 95.0%, 90.0%, 77.9%, 69.6%, respectively for MIAS-manual, MIAS-auto, DDSM and OPTIMUM dataset. While comparing to other topological modelling methods for microcalcification classifications on the DDSM dataset using the kNN classifier; Strange et al. [22] attained classification accuracy of 80.0% for a set of 300 cases and modelled the relationship between microcalcification regions in the form of mereotopological barcodes. Similarly, Chen et al. [44] utilized the spatial connectivity relationship for building a multi-scale graph model where two nodes are linked as edge if the corresponding microcalcifications overlap each other. The method obtained a classification accuracy of 85.2% ± 5.7% for a set of 289 cases. Later Suhail et al. [45] developed a topological model using the binary tree properties and classified the clusters as benign/malignant based on the height of the tree and obtained an accuracy of 55.0% for whole dataset and 91.0% for a subset of 129 images. In-order to investigate the strength of topological modelling for microcalcification classification, Ashiru et al. [56] conducted a study to compare the topological modelling by Chen et al. [44] and location based classification by [59] and found topological models performed better in explaining the microcalcification clusters. Unlike other toplogical models discussed, we utilize the distributional arrangement of microcalcifications in a cluster to form sub-clusters to represent the relative arrangement of benign and malignant microcalcifications and obtained a classification accuracy of 86.47% ± 1.30% for a set of 289 cases.

Incorrect Classification Results. Though the proposed approach can classify most of the cases correctly, there were misclassified instances like the mammographic patches shown in Fig. 6. The top row ROI was misclassified as a malignant case by the proposed approach where the microcalcifications were closely distributed though they were larger in size and so they merged easily to become a single cluster with minimum scaling which contradicts the assumption that benign calcifications are widely spread and needed a higher number of scales before they overlap. This was unexpected for the proposed approach where we assumed that for benign cases the microcalcifications were widely spread. Similarly, the second row represents a malignant ROI reported as benign because the microcalcifications were widely distributed though they were of small size. So with a limited number of scales, the merging of microcalcifications were not possible which led to the extraction of features similar to benign properties.

From the comparative results between the datasets, it can be concluded that the method needs a explicitly detected microcalcification cluster and the dataset resolution is a factor to be considered as the resolution of the MIAS and DDSM datasets was similar, (50 μm per pixel) for the OPTIMAM dataset, the resolution was 70 μm per pixel.

5. Conclusion and future work

Detection and classification of benign and malignant microcalcifications is an important issue for CAD systems as it can assist in the early diagnosis and treatment of breast cancer. CAD systems with great accuracy for detection and classification can act as a second reader of mammographic images and can reduce incorrect treatment.

In this paper we have introduced a novel approach considering the topological distribution of microcalcifications in mammogram ROIs using a multi-scale approach. This takes the clinical description of microcalcification distribution into account for the cluster classification process. The results obtained are similar to techniques reported in the literature for the MIAS and DDSM datasets for the KNN classifier.

The proposed algorithm was implemented for a specific number of scales and the optimum number of scales is an important factor which will be investigated in the future. Similarly, additional datasets will be considered to evaluate the algorithm. Simultaneously, the effect of the segmentation method on the classification results will be studied in more detail. In addition to the microcalcification distribution features, the surrounding tissue characteristic features will be extracted to investigate the classification efficiency as future work.

References

[1] F. Bray, J. Ferlay, I. Soerjomataram, R.L. Siegel, L.A. Torre, A. Jemal, Global cancer statistics 2018: globocan estimates of incidence and mortality worldwide for 36 cancers in 185 countries, CA A Cancer J. Clin. 68 (6) (2018) 394–424.
[2] M. Elter, A. Horsch, Cadx of mammographic masses and clustered microcalcifications: a review, Med. Phys. 36 (6) (2009) 2052–2068.
[3] K.J. Wernli, E.J.A. Bowles, S. Haneuse, J.G. Elmore, D.S. Buist, Timing of follow-up after abnormal screening and diagnostic mammograms, Am. J. Manag. Care 17 (2) (2011) 162.
[4] J. Hernández-Capistrán, J.F. Martínez-Carballido, Thresholding methods review for microcalcifications segmentation on mammography images in obvious, subtle, and cluster categories, in: 2016 13th International Conference on Electrical Engineering, Computing Science and Automatic Control (CCE), IEEE, 2016, pp. 1–6.
[5] A. Tiedeu, C. Daul, A. Kentsop, P. Graebling, D. Wolf, Texture-based analysis of clustered microcalcifications detected on mammograms, Digit. Signal Process. 22 (1) (2012) 124–132.
[6] K. Ganesan, R.U. Acharya, C.K. Chua, L.C. Min, B. Mathew, A.K. Thomas, Decision support system for breast cancer detection using mammograms, Proc. Inst. Mech. Eng. H J. Eng. Med. 227 (7) (2013) 721–732.
[7] L. Wei, Y. Yang, R.M. Nishikawa, Y. Jiang, A study on several machine-learning methods for classification of malignant and benign clustered microcalcifications, IEEE Trans. Med. Imaging 24 (3) (2005) 371–380.
[8] M.K. Shetty, Screening for breast cancer with mammography: current status and an overview, Indian J. Surg. Oncol. 1 (3) (2010) 218–223.

[9] R. Wilson, D. Asbury, J. Cooke, M. Michell, J. Patnick, Clinical Guidelines for Breast Cancer Screening Assessment, vol. 49, NHSBSP publication, 2001.

[10] V.M. Rao, D.C. Levin, L. Parker, B. Cavanaugh, A.J. Frangos, J.H. Sunshine, How widely is computer-aided detection used in screening and diagnostic mammography? J. Am. Coll. Radiol. 7 (10) (2010) 802–805.

[11] S. Zhang, H. Chen, J. Li, Segmentation of microcalcifications in mammograms based on multi-resolution region growth and image difference, in: 2011 4th International Congress on Image and Signal Processing vol. 3, IEEE, 2011, pp. 1273–1276.

[12] E.L. Henriksen, J.F. Carlsen, I.M. Vejborg, M.B. Nielsen, C.A. Lauridsen, The efficacy of using computer-aided detection (cad) for detection of breast cancer in mammography screening: a systematic review, Acta Radiol. 60 (1) (2019) 13–18.

[13] A. Jalalian, S. Mashohor, R. Mahmud, B. Karasfi, M.I.B. Saripan, A.R.B. Ramli, Foundation and methodologies in computer-aided diagnosis systems for breast cancer detection, EXCLI J. 16 (2017) 113.

[14] J.D. Keen, J.M. Keen, J.E. Keen, Utilization of computer-aided detection for digital screening mammography in the United States, 2008 to 2016, J. Am. Coll. Radiol. 15 (1) (2018) 44–48.

[15] M.G. Marmot, D. Altman, D. Cameron, J. Dewar, S. Thompson, M. Wilcox, The benefits and harms of breast cancer screening: an independent review, Br. J. Canc. 108 (11) (2013) 2205.

[16] R.M. Nishikawa, Current status and future directions of computer-aided diagnosis in mammography, Comput. Med. Imag. Graph. 31 (4–5) (2007) 224–235.

[17] K. Doi, Computer-aided diagnosis in medical imaging: achievements and challenges, in: World Congress on Medical Physics and Biomedical Engineering, September 7-12, 2009, Springer, Munich, Germany, 2009, 96–96.

[18] Y. Gao, K.J. Geras, A.A. Lewin, L. Moy, New frontiers: an update on computer-aided diagnosis for breast imaging in the age of artificial intelligence, Am. J. Roentgenol. 212 (2) (2019) 300–307.

[19] H.-D. Cheng, X. Cai, X. Chen, L. Hu, X. Lou, Computer-aided detection and classification of microcalcifications in mammograms: a survey, Pattern Recognit. 36 (12) (2003) 2967–2991.

[20] A.M. Abdel-Zaher, A.M. Eldeib, Breast cancer classification using deep belief networks, Expert Syst. Appl. 46 (2016) 139–144.

[21] H. Soltanian-Zadeh, F. Rafiee-Rad, S. N. D, Comparison of multiwavelet, wavelet, haralick, and shape features for microcalcification classification in mammograms, Pattern Recognit. 37 (10) (2004) 1973–1986.

[22] H. Strange, Z. Chen, E.R. Denton, R. Zwiggelaar, Modelling mammographic microcalcification clusters using persistent mereotopology, Pattern Recognit. Lett. 47 (2014) 157–163.

[23] P.L.A. Hernández, T.T. Estrada, A.L. Pizarro, M.L.D. Cisternas, C.S. Tapia, Breast calcifications: description and classification according to bi-rads 5th edition, Rev. Chil. Radiol. 22 (2016) 80–91.

[24] A. Papadopoulos, D.I. Fotiadis, A. Likas, Characterization of clustered microcalcifications in digitized mammograms using neural networks and support vector machines, Artif. Intell. Med. 34 (2) (2005) 141–150.

[25] J. Mordang, A. Gubern-Mérida, A. Bria, F. Tortorella, R. Mann, M. Broeders, G. den Heeten, N. Karssemeijer, The importance of early detection of calcifications associated with breast cancer in screening, Breast Canc. Res. Treat. 167 (2) (2018) 451–458.

[26] E. Sakka, A. Prentza, D. Koutsouris, Classification algorithms for microcalcifications in mammograms, Oncol. Rep. 15 (4) (2006) 1049–1055.

[27] S.-K. Lee, P.-C. Chung, C.-I. Chang, C.-S. Lo, T. Lee, G.-C. Hsu, C.-W. Yang, Classification of clustered microcalcifications using a shape cognitron neural network, Neural Netw. 16 (1) (2003) 121–132.

[28] J.Y. Lo, M.A. Gavrielides, M.K. Markey, J.L. Jesneck, Computer-aided classification of breast microcalcification clusters: merging of features from image processing and radiologists, in: Medical Imaging 2003: Image Processing vol. 5032, International Society for Optics and Photonics, 2003, pp. 882–890.

[29] M. Ciecholewski, Microcalcification segmentation from mammograms: a morphological approach, J. Digit. Imaging 30 (2) (2017) 172–184.

[30] B. Singh, M. Kaur, An approach for classification of malignant and benign microcalcification clusters, Sādhanā 43 (3) (2018) 39.

[31] A. Karahaliou, S. Skiadopoulos, I. Boniatis, P. Sakellaropoulos, E. Likaki, G. Panayiotakis, L. Costaridou, Texture analysis of tissue surrounding microcalcifications on mammograms for breast cancer diagnosis, Br. J. Radiol. 80 (956) (2007) 648–656.

[32] I. Zyout, I. Abdel-Qader, An improvement of texture-based classification of microcalcification clusters in mammography using pso-svm approach, in: The 5th International Conference on Communications, Computers and Applications (MIC-Cca2012), IEEE, 2012, pp. 7–11.

[33] I. Zyout, I. Abdel-Qader, Classification of microcalcification clusters via pso-knn heuristic parameter selection and glcm features, Int. J. Comput. Appl. 31 (2) (2011) 34–39.

[34] E. Malar, A. Kandaswamy, D. Chakravarthy, A.G. Dharan, A novel approach for detection and classification of mammographic microcalcifications using wavelet analysis and extreme learning machine, Comput. Biol. Med. 42 (9) (2012) 898–905.

[35] C. Abirami, R. Harikumar, S.S. Chakravarthy, Performance analysis and detection of micro calcification in digital mammograms using wavelet features, in: 2016 International Conference on Wireless Communications, Signal Processing and Networking (WiSPNET), IEEE, 2016, pp. 2327–2331.

[36] K.A. Batchelder, A.B. Tanenbaum, S. Albert, L. Guimond, P. Kestener, A. Arneodo, A. Khalil, Wavelet-based 3d reconstruction of microcalcification clusters from two mammographic views: new evidence that fractal tumors are malignant and euclidean tumors are benign, PLoS One 9 (9) (2014).

[37] V. Gowri, K. Valluvan, V.V. Chamundeeswari, Automated detection and classification of microcalcification clusters with enhanced preprocessing and fractal analysis, Asian Pac. J. Cancer Prev. APJCP 19 (11) (2018) 3093.

[38] A. Shirazinodeh, H.A. Noubari, H. Rabbani, A.M. Dehnavi, Detection and classification of breast cancer in wavelet sub-bands of fractal segmented cancerous zones, J. Med. Signals Sens. 5 (3) (2015) 162.

[39] A.J. Bekker, H. Greenspan, J. Goldberger, A multi-view deep learning architecture for classification of breast microcalcifications, in: Biomedical Imaging (ISBI), 2016 IEEE 13th International Symposium on, IEEE, 2016, pp. 726–730.

[40] J. Wang, Y. Yang, A context-sensitive deep learning approach for microcalcification detection in mammograms, Pattern Recognit. 78 (2018) 12–22.

[41] J. Wang, R.M. Nishikawa, Y. Yang, Global detection approach for clustered microcalcifications in mammograms using a deep learning network, J. Med. Imaging 4 (2) (2017) 024501.

[42] P. Xi, C. Shu, R. Goubran, Abnormality detection in mammography using deep convolutional neural networks. 1803.01906.

[43] Z. Chen, H. Strange, E. Denton, R. Zwiggelaar, Analysis of mammographic microcalcification clusters using topological features, in: International Workshop on Digital Mammography, Springer, 2014, pp. 620–627.

[44] Z. Chen, H. Strange, A. Oliver, E.R. Denton, C. Boggis, R. Zwiggelaar, Topological modeling and classification of mammographic microcalcification clusters, IEEE (Inst. Electr. Electron. Eng.) Trans. Biomed. Eng. 62 (4) (2015) 1203–1214.

[45] Z. Suhail, E.R. Denton, R. Zwiggelaar, Tree-based modelling for the classification of mammographic benign and malignant micro-calcification clusters, Multimed. Tools Appl. 77 (5) (2018) 6135–6148.

[46] M. Heath, K. Bowyer, D. Kopans, R. Moore, P. Kegelmeyer, The digital database for screening mammography, Digit. Mammogr. (2000) 431–434.

[47] J. Suckling, J. Parker, D. Dance, S. Astley, I. Hutt, C. Boggis, I. Ricketts, E. Stamatakis, N. Cerneaz, S. Kok, T. P, The mammographic image analysis society digital mammogram database, in: Exerpta Medica. International Congress Series, vol. 1069, 1994, pp. 375–378.

[48] A. Oliver, A. Torrent, X. Lladó, M. Tortajada, L. Tortajada, M. Sentís, J. Freixenet, R. Zwiggelaar, Automatic microcalcification and cluster detection for digital and digitised mammograms, Knowl. Based Syst. 28 (2012) 68–75.

[49] N. Alam, A. Oliver, E.R. Denton, R. Zwiggelaar, Automatic segmentation of microcalcification clusters, in: Annual Conference on Medical Image Understanding and Analysis, Springer, 2018, pp. 251–261.

[50] S. Lele, J.T. Richtsmeier, Euclidean distance matrix analysis: a coordinate-free approach for comparing biological shapes using landmark data, Am. J. Phys. Anthropol. 86 (3) (1991) 415–427.

[51] P. Soille, Morphological Image Analysis: Principles and Applications, Springer Science & Business Media, 2013.

[52] R.O. Duda, P.E. Hart, D.G. Stork, Pattern Classification, John Wiley & Sons, 2012.

[53] K. Hajian-Tilaki, Receiver operating characteristic (roc) curve analysis for medical diagnostic test evaluation, Casp. J. Intern. Med. 4 (2) (2013) 627.

[54] Y. Ma, P.C. Tay, R.D. Adams, J.Z. Zhang, A novel shape feature to classify microcalcifications, in: Image Processing (ICIP), IEEE, 2010, pp. 2265–2268.

[55] J. Ren, Ann vs. svm: which one performs better in classification of mccs in mammogram imaging, Knowl. Based Syst. 26 (2012) 144–153.

[56] O. Ashiru, R. Zwiggelaar, Classification of mammographic microcalcification clusters using a combination of topological and location modelling, in: Image Processing Theory Tools and Applications (IPTA), IEEE, 2016, pp. 1–6.

[57] J. Dheeba, S.T. Selvi, Classification of malignant and benign microcalcification using svm classifier, in: Emerging Trends in Electrical and Computer Technology (ICETECT), IEEE, 2011, pp. 686–690.

[58] M. George, E.R.E. Denton, R. Zwiggelaar, Topological connected chain modelling for classification of mammographic microcalcification, in: Computer Graphics and Visual Computing (CGVC), The Eurographics Association, 2018.

[59] I.I. Andreadis, G.M. Spyrou, K.S. Nikita, A cadx scheme for mammography empowered with topological information from clustered microcalcifications' atlases, IEEE J. Biomed. Health Inf. 19 (1) (2015) 166–173.